Journal of Translational Medicine

RESEARCH

Open Access

Single-cell atlas of hepatic cellular plasticity and immune niche reprogramming in liver cirrhosis

Qing Zhang[1†], Nan Zhou[3†], Xiuli Kan[4†], Zhicheng Zhang[1], Yi Fang[1], Han Liu[1] and Ying Chen[1,2*]

Abstract

Background Cirrhosis is a severe liver disease characterized by inflammation, fibrosis, and immune dysregulation. This study exploits publicly available single-cell sequencing datasets to decipher disease-relevant specific immune cell subtypes, their gene expression profiles and altered transcription factor activity in cirrhosis, aiming to understand their roles in disease onset and progression.

Methods To investigate the dynamic changes and underlying mechanisms of immune cells in cirrhosis, we employed a comprehensive bioinformatics approach integrating several advanced tools and analytical methods. Single-cell RNA sequencing data were processed and analyzed using Seurat for cell clustering and annotation. Monocle was used for pseudotime trajectory analysis to explore cellular differentiation pathways. CellChat enabled the assessment of cell–cell communication networks among immune populations. Additionally, we conducted single-cell regulatory network inference to identify key transcriptional regulators. Immune response enrichment analysis (IREA) was performed to evaluate immune-related functional pathways, providing deeper insights into the immune landscape and disease progression in cirrhosis.

Results We analyzed 35,017 cells, identifying 21 clusters and 12 major immune cell types. Macrophages, $CD4^+$ T cells, and NK cells showed notable shifts in proportion in cirrhosis, suggesting key roles in disease progression. Pseudotime analysis revealed core macrophage and $CD4^+$ T-cell subpopulations linked to cirrhosis. Functional analysis showed enrichment of IFN-α, IFN-β, and IL-1β in cirrhotic immune cells, primarily regulated by *ETS2* and *THRA*. Fibroblast-mediated intercellular communication was enhanced, especially via increased macrophage migration inhibitory factor (MIF) signaling with B cells, indicating potential therapeutic targets in cytokine pathways and transcriptional regulation.

Conclusion The analysis revealed three key axes influencing disease-related immune regulation: TNF-α/*ETS2*-driven polarization of macrophages toward a Mac-d phenotype, IL-1α/β/*THRA*-associated polarization of $CD4^+$ T cells toward

†Qing Zhang, Nan Zhou and Xiuli Kan contributed equally to this work.

*Correspondence:
Ying Chen
ychen@ahmu.edu.cn

Full list of author information is available at the end of the article

© The Author(s) 2026. **Open Access** This article is licensed under a Creative Commons Attribution-NonCommercial-NoDerivatives 4.0 International License, which permits any non-commercial use, sharing, distribution and reproduction in any medium or format, as long as you give appropriate credit to the original author(s) and the source, provide a link to the Creative Commons licence, and indicate if you modified the licensed material. You do not have permission under this licence to share adapted material derived from this article or parts of it. The images or other third party material in this article are included in the article's Creative Commons licence, unless indicated otherwise in a credit line to the material. If material is not included in the article's Creative Commons licence and your intended use is not permitted by statutory regulation or exceeds the permitted use, you will need to obtain permission directly from the copyright holder. To view a copy of this licence, visit http://creativecommons.org/licenses/by-nc-nd/4.0/.

a T4-c phenotype, and enhancement of the fibroblast-to-B-cell MIF signaling axis. This network offers valuable insights and potential therapeutic targets for advancing cirrhosis research and clinical treatment.

Highlights

- The TNF-α/*ETS2* axis drives macrophage polarization to a Mac-d phenotype.
- The IL-1α/β/*THRA* axis mediates $CD4^+$ T cell polarization to a T4-c phenotype.
- The fibroblast-to-B-cell MIF signaling axis is enhanced in cirrhosis.

Keywords Cirrhosis, Immune cell phenotype, Single-cell sequencing, Immune response enrichment analysis, Cell polarization

Graphical abstract

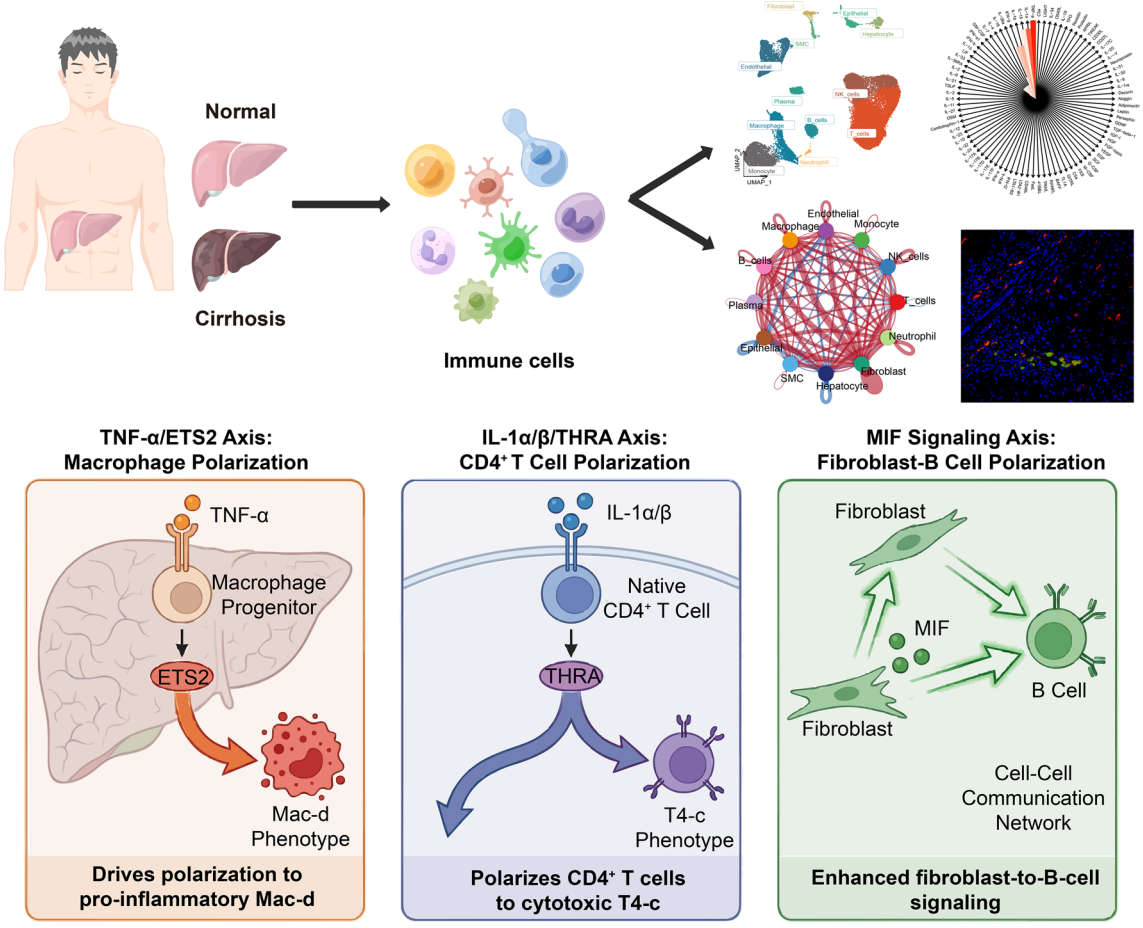

Background

Globally, the age-standardized death rate of liver cirrhosis is approximately 18 deaths per 100,000 people, translating to the 12th leading cause of death [1, 2]. Progressive fibrosis and the development of regenerating nodules are the major pathological hallmarks [3, 4], in addition to jaundice [5, 6], ascites [7, 8] and hepatic encephalopathy [9]. Furthermore, cirrhosis can significantly heighten the risk of developing hepatocellular carcinoma (HCC), as 80–90% of HCC patients are comorbid with cirrhosis [10–12]. Current treatments for liver cirrhosis primarily involve symptom-based therapies, complication management, and investigations of underlying causes, such as viral hepatitis or alcohol misuse, to prevent persistent damage to the liver [13, 14]. Nevertheless, these methods do not address advanced fibrosis reversal or liver function restoration, highlighting the need to investigate new perspectives on the cellular mechanisms of cirrhosis for potential novel therapeutic interventions.

The pathogenesis of cirrhosis is closely linked to a dynamic and heterogeneous immune response, with both innate and adaptive immune cells playing pivotal roles in driving inflammation, fibrosis, and immune dysregulation [10, 15, 16]. However, conventional bulk transcriptomic approaches have provided limited resolution in dissecting the complex cellular heterogeneity

of the liver immune microenvironment during cirrhosis. For example, activated Kupffer cells and recruited monocyte-derived macrophages release TGF-β1, as well as proinflammatory cytokines and chemokines, such as TNF, IL-1β or CCL2, which orchestrate the stimulation of hepatic stellate cells (HSCs) and the recruitment of inflammatory cells to the tumor microenvironment [17]. Intrahepatic B cells also contribute to fibrogenesis by secreting immunoglobulin [18].

In recent years, single-cell omics has significantly increased our knowledge of key molecular and cellular factors, immensely contributing to targeted therapy development for life-threatening liver diseases [19–21]. For example, MacParland et al. first constructed a single-cell atlas of the healthy human liver, systematically identifying diverse immune cell subtypes and laying the foundation for understanding the hepatic immune microenvironment [22]. Ramachandran et al. further elucidated the interaction mechanisms between hepatic stellate cells and immune cells in end-stage liver fibrotic tissue, revealing key signaling pathways within the fibrotic microenvironment [23]. However, existing studies have focused mainly on healthy liver or end-stage fibrotic tissue without systematically delineating the functional reprogramming characteristics of immune cell subsets during the process of liver cirrhosis. Specifically, there is a lack of integrated research on the polarization states, transcriptional regulatory networks, and communication patterns of key immune cells, such as macrophages, T cells, NK cells, monocytes, and B cells, driven by cytokines.

To address this gap, we performed an integrated analysis using publicly available single-cell RNA sequencing data and integrated immune response enrichment analysis (IREA) and single-cell regulatory network inference and clustering (SCENIC) to systematically delineate immune cell polarization characteristics, dynamic changes in transcription factors, and reshaping of cell communication patterns in liver cirrhosis, providing new systematic evidence for elucidating the reprogramming mechanisms of the immune microenvironment in liver cirrhosis.

Methods

Data download and processing

ScRNA-seq data for cirrhosis patients were obtained from the Gene Expression Omnibus (GEO) database under accession number GSE168933, which includes 23 liver tissue samples, comprising five cirrhotic patient samples and seven noncirrhotic samples. We excluded any other samples without any clear pathological identification from the analysis to ensure the scientific rigor of the grouping and the compatibility of the samples. The raw sequencing data were processed via the Seurat package (version 4.2.0) in R [24]. The initial quality control steps included removal of cells with no detectable gene expression, retention of cells expressing between 200 and 4000 genes, exclusion of cells with unique molecular identifier (UMI) counts exceeding 20,000, and exclusion of cells with red blood cell (RBC) gene expression greater than 1%. Data normalization was carried out via the "normalizedata" function from the Seurat R (version 2.25.0) package. Highly variable genes were identified in each dataset on the basis of mean expression and dispersion metrics. Principal component analysis (PCA) was then conducted, and significant principal components (PCs) were selected for downstream graph-based clustering. To correct for batch effects across samples, the Harmony algorithm was applied. Clustering was conducted via the "FindClusters" function, yielding 21 distinct clusters on the basis of 19 PCs at a resolution of 0.8 and employing a shared nearest neighbor (SNN) modularity optimization algorithm. Visualization of cell clusters was achieved using Uniform Manifold Approximation and Projection (UMAP) via the "RunUMAP" function to visualize cell clustering. Differentially expressed genes (DEGs) for each cluster were identified using the "FindAllMarkers" function with default parameters. Cluster-specific biomarkers were subsequently determined to characterize and quantify distinct cell populations. Unless explicitly indicated, all analytical procedures, such as cell clustering, identification of cellular subpopulations, and functional enrichment, along with their associated results and figures, were performed using a pooled dataset comprising all samples.

Identification of DEGs

Exploring the gene expression levels of key cells at the single-cell level between the cirrhosis and control groups based on identified key cells. Differential analysis was conducted using the R package limma (version 3.50.0), resulting in the identification of DEGs in key cells between the cirrhosis and control groups [25]. Genes meeting the criteria of $|\log FC| > 0.25$ and p value < 0.05 were selected for further investigation.

Pseudotime trajectory analysis

Single-cell pseudotime trajectories were conducted using Monocle 2 (version 3.3.5) [26]. Monocle 2 utilizes a user-defined gene list to perform reverse graph embedding and generate a pseudotime trajectory, elucidating branching and linear differentiation processes. For key cell populations, the original count data were normalized using cell-specific size factors. Pseudotime trajectories were constructed using highly dispersed and expressed genes (with a dispersion estimate ≥ 1 and average expression ≥ 0.1) [27]. Default parameters were selected for the DDRTree algorithm. Branch expression

analysis modeling (BEAM) implemented in Monocle 2 was employed to further investigate these branching events, aiding in the identification of genes with significant branch-dependent expression [26]. Branch-dependent expression patterns were visualized with heatmaps using Monocle 2.

Pathway enrichment analysis

GO and KEGG pathway enrichment analyses were conducted on differentially expressed genes in cirrhosis using the Gene Ontology (GO) [28], which includes Biological Process (BP), Molecular Function (MF), and Cellular Component (CC) analyses, and the Kyoto Encyclopedia of Genes and Genomes (KEGG) [29], a bioinformatics resource for identifying enriched and significantly altered metabolic pathways in gene lists. The analysis was performed using the R software package "clusterProfiler (version 4.2.2)" with a significance threshold of $p < 0.05$ [30].

Single-cell regulatory network analysis

To identify key transcription factors (TFs) in specific cell types in liver cirrhosis, we conducted cis-regulatory analysis using pySCENIC (version 0.11.2), a tool that infers gene regulatory networks based on coexpression and DNA motif analysis [31]. A regulatory network consisting of TFs and their target genes was established. The AUCell module within pySCENIC was utilized to analyze the regulon activity, identifying active regulons using default AUCell thresholds. Furthermore, the scaled expression of regulon activity was used to generate a heatmap. Cell type-specific regulon specificity scores (RSS) were calculated to further characterize the specificity of each cell type's regulons.

Cell–cell communication analysis

The CellChat object was created using the "CellChat" R package (version 3.3.5) based on the UMI count matrix for each group (cirrhosis and control) (https://www.github.com/sqjin/CellChat) [32]. Cell–cell communication was analyzed using the "CellChatDB.human" ligand–receptor interaction database as the reference, with default parameters. The "mergeCellChat" function was utilized to combine CellChat objects from each group for comparison of interaction totals and strengths. The statistical significance of communication strength differences between cirrhotic and control groups was assessed by a permutation test ($n = 1000$) with a significance level set at $p < 0.05$. Effect sizes of intergroup differences were quantified using standardized mean difference (Cohen's d) or $\log_2$ fold change ($\log_2$FC). For key signaling pathways between fibroblasts and immune cells, ligand–receptor pairs related to the MIF pathway (MIF-CD74, MIF-CD44, MIF-CXCR4) were extracted, and pathway activation was evaluated by incorporating the expression levels of downstream signaling genes (e.g., NF-κB, *IL1B*, *JUN*). The "netVisual_diffInteraction" function was used to visualize differences in interaction quantity or strength between different cell types. Communication probabilities and statistical results were presented as heatmaps and boxplots annotated with permutation test p values and effect sizes. Finally, the "netVisual_bubble" and "netVisual_aggregate" functions were applied to visualize the distribution of intergroup signaling gene expression.

IREA

The immune response enrichment analysis (IREA), developed by Ang Cui et al., is a computational tool designed to infer cytokine activity and immune cell polarization across various immune processes using transcriptomic datasets [33]. This approach can identify over 66 cytokine-driven polarization states in immune cell populations, including previously uncharacterized subsets. By analyzing upregulated genes in key immune cell subpopulations that were differentially expressed between the cirrhosis and control groups ($|\log_2\text{Fold Change}| > 0.25$, $p < 0.05$), we applied IREA to identify the predominant response factors secreted by these cells and to determine their polarization states. The polarization of each subpopulation was interpreted based on the functional axis exhibiting the highest and most statistically significant enrichment score.

Histological analysis of human liver tissues

Human liver tissue samples obtained from the Second Affiliated Hospital of Anhui Medical University were sectioned at 3–5 μm and subjected to hematoxylin and eosin (H&E) staining for histological assessment, as well as Masson's trichrome staining for collagen identification. The stained sections were subsequently observed under a light microscope to analyze morphological alterations and extracellular matrix accumulation.

Immunofluorescence staining

Immunofluorescence was performed on paraffin-embedded sections. The sections were deparaffinized, rehydrated, blocked, and incubated with primary antibodies at 37 °C. After washing, the sections were incubated with fluorescence-conjugated secondary antibodies. Nuclei were stained with DAPI. Images were captured using a Leica fluorescence microscope.

Statistical analysis

The statistical analysis in this study was conducted using R software version 4.1.2. The Spearman correlation test was employed to infer the correlation between two parameters. The Wilcoxon test was used to compare differences between two groups, while the Kruskal–Wallis

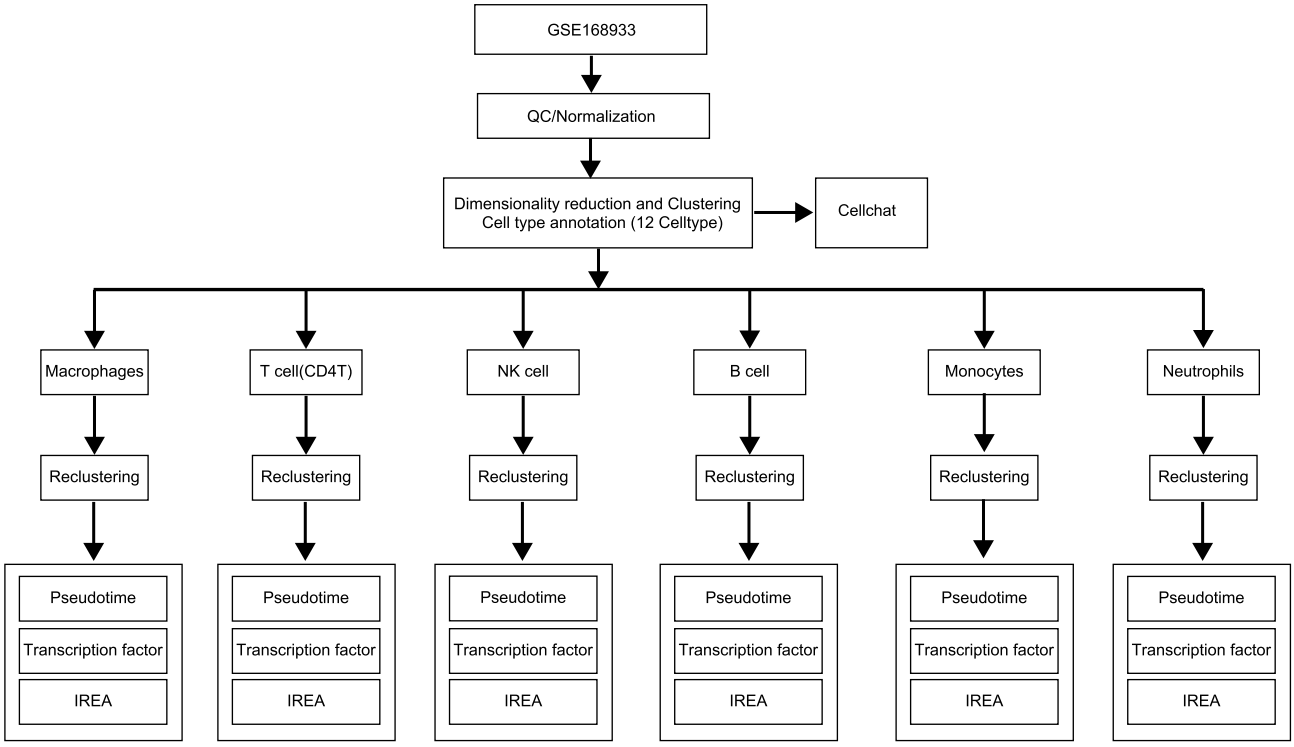

Fig. 1 A flow diagram of the liver cirrhosis dataset analysis and outcomes

test was utilized to compare differences among three or more groups. A two-tailed *p* value less than 0.05 was considered statistically significant.

Results

The abundance of monocytes, endothelial cells, and macrophages is altered in liver cirrhosis

To elucidate the immune landscape underlying cirrhosis development, we employed scRNA-seq to comprehensively characterize immune cell heterogeneity in liver tissue samples using the GSE168933 dataset (Fig. 1). After performing quality control filtering and removing doublets, a total of 35,017 high-quality cells were retained for downstream analysis. The cells were grouped into 21 clusters (Fig. 2A), which were subsequently annotated based on canonical gene expression signatures and known cell type-specific markers (Table S1, Fig. 2C). As shown in Fig. 2B, we identified 12 major cell types, including T cells, NK cells, monocytes, endothelial cells, macrophages, B cells, plasma cells, epithelial cells, smooth muscle cells (SMCs) and neutrophils, through UMAP plotting.

Figure 2D and Fig. S1 show the proportional distributions of these cell types across cirrhotic and noncirrhotic samples. Notably, the relative abundances of monocytes, endothelial cells, and macrophages significantly differed between the two conditions, suggesting that these cell types may play key roles in the pathophysiology and progression of liver cirrhosis.

TNF-α mediates macrophage polarization in liver cirrhosis

To gain a deeper understanding of macrophage heterogeneity, we performed focused reclustering of the macrophage population using the top 10 PCs at a resolution of 0.2, resulting in the identification of six distinct macrophage clusters (Fig. 3A and S2A). To investigate the functional diversity of these subpopulations, differentiation trajectories were plotted for pseudotime (Fig. 3B), cellular states (Fig. 3C), cell types (Fig. S2B), and diseased state (Fig. S2C). Notably, the trajectory revealed two branch points, delineating five discrete cell states (Fig. 3C). Among them, the Macrophage_3 cluster was predominantly associated with States 4 and 5, suggesting a dominant role in late-stage macrophage differentiation. Notably, we observed distinct differentiation patterns between the cirrhotic and noncirrhotic groups, particularly within State 5, where Macrophage_3 displayed enhanced differentiation in the cirrhotic group (Fig. S2D-E). Further analysis of the three branches stemmed from branch point 2 revealed functional variances such that cells in the prebranch (State 1, Cluster 1) were enriched in pathways related to "negative regulation of immune system process," "complement activation," and "synapse pruning." In contrast, branch 2 (State 5, Cluster 2) was enriched in "phosphatidylcholine metabolic

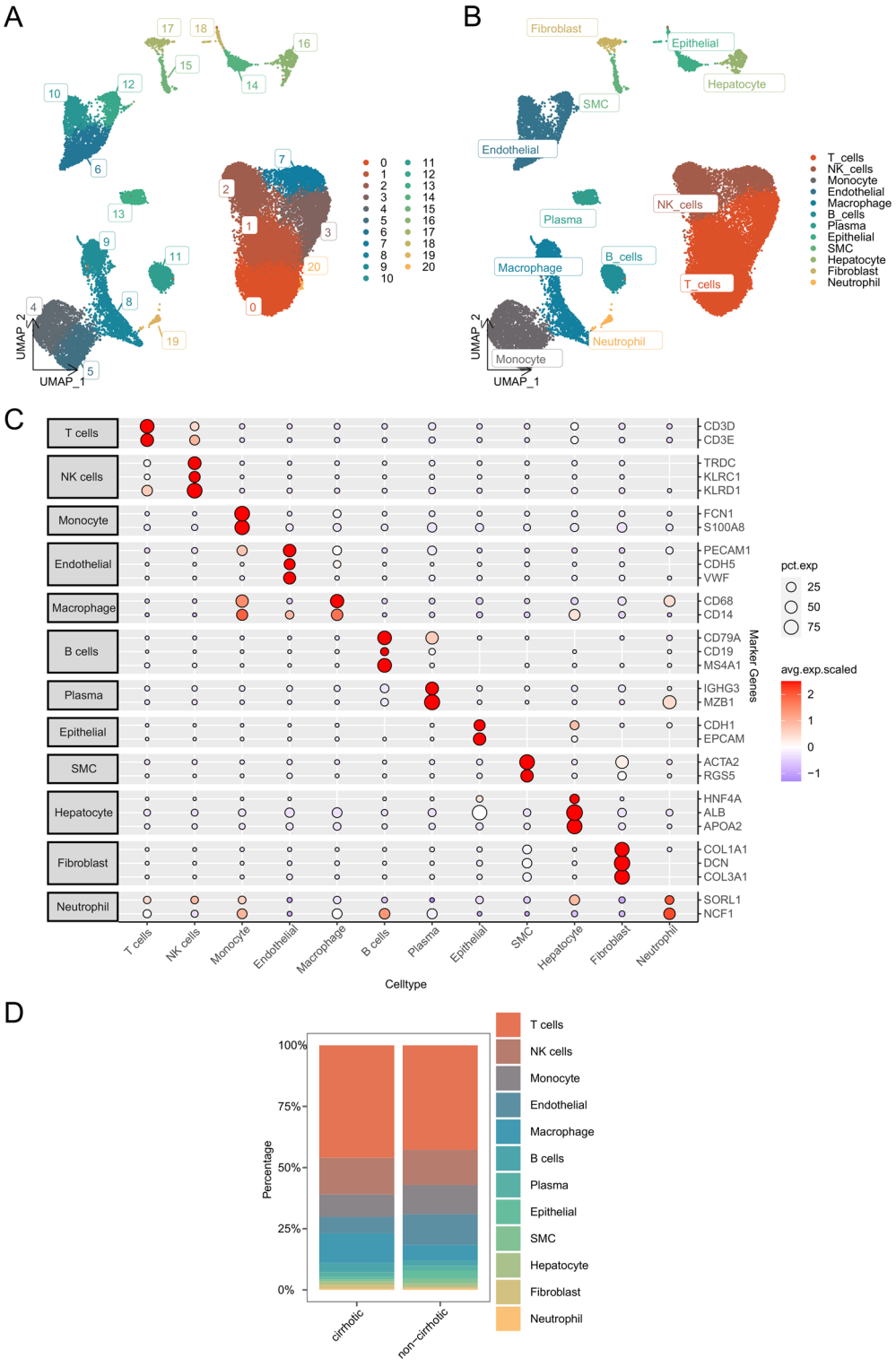

Fig. 2 The annotation and visualization of the cellular environment in cirrhosis. **A**) UMAP visualization illustrated the distribution of 21 cell subtypes in the cirrhotic and control groups. **B**) The UMAP plot displayed the annotation results and distribution of 12 major cell types in cirrhosis. **C**) Expression of marker genes in each cell type. **D**) Stacked bar graphs depicted the comparison of cell type proportions between the cirrhotic and control groups

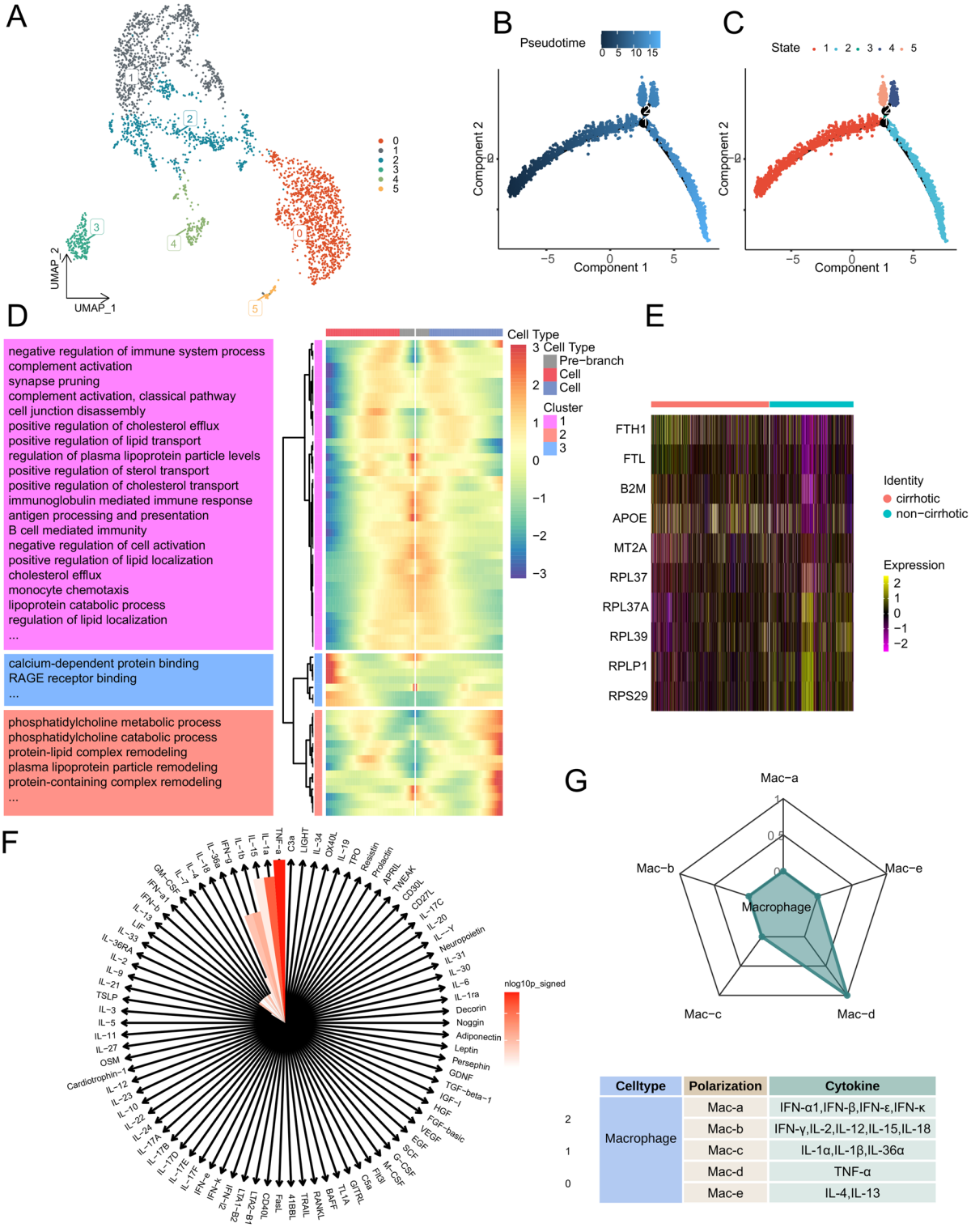

Celltype	Polarization	Cytokine
Macrophage	Mac-a	IFN-α1,IFN-β,IFN-ε,IFN-κ
	Mac-b	IFN-γ,IL-2,IL-12,IL-15,IL-18
	Mac-c	IL-1α,IL-1β,IL-36α
	Mac-d	TNF-α
	Mac-e	IL-4,IL-13

Fig. 3 Macrophage reclustering, pseudotime trajectory reconstruction, and functional enrichment profiling. **A**) UMAP visualization of the distribution of macrophage subtypes. **B**) Pseudotime trajectory coloring transitions from dark blue to light blue. **C**) Monocle2 divided the pseudotime trajectory into 5 distinct states. **D**) Heatmap displayed the DEGs of different branches (cell fates). Enriched GO pathways of different gene clusters are shown on the left side of the heatmap. **E**) Heatmap displaying 10 significant DEGs of Macrophage_3 between the cirrhotic and non-cirrhotic groups. **F**) Cytokine enrichment plot of Macrophage_3 in cirrhosis. **G**) Radar plot and immune checkpoint card depicting the polarization of macrophages in cirrhosis

process," whereas branch 1 (State 4, Cluster 3) exhibited high expression of genes involved in "calcium-dependent protein binding" (Fig. 3D and Table S2). We next performed differential gene expression analysis on the Macrophage_3 subset between the cirrhotic and noncirrhotic groups, identifying 411 DEGs ($|\log_2 FC| > 0.25$, $p < 0.05$). The top 10 DEGs were visualized using bubble and heatmaps to highlight their expression changes across key immune cell populations (Fig. 3E and S2F). GO enrichment analysis of these DEGs displayed significant enrichment in BPs such as cytoplasmic translation, rRNA processing, and ribosome biogenesis; CCs including cytosolic ribosome and ribosomal subunit; and MFs such as structural constituent of ribosome, rRNA binding, and cadherin binding (Fig. S2G and Table S3). KEGG pathway analysis further highlighted enrichment in pathways related to endocytosis, phagosome formation, ribosome function, and protein processing in the endoplasmic reticulum, as well as disease-associated pathways including allograft rejection and Epstein–Barr virus infection (Fig. S2H and Tables S4–5). To further assess the polarization states of macrophages, IREA was performed on the genes whose expression was significantly upregulated in the cirrhotic group. Radar plot visualization revealed that macrophages in the cirrhotic group predominantly exhibited a Mac-d polarization profile (M1-like proinflammatory) (Fig. 3F), with increased expression of the proinflammatory cytokine TNF-α (Fig. 3G). HE and Masson staining confirmed significant collagen deposition in the cirrhotic group (Fig. 4A, B). Immunofluorescence analysis revealed markedly upregulated TNF-α expression in the cirrhotic group, with evident colocalization with the macrophage marker CD68 (Fig. 4C–E).

Collectively, these findings suggest that hepatic macrophages in cirrhosis undergo functional reprogramming, which is marked by late-stage differentiation (Macrophage_3 dominance). Proinflammatory Mac-d polarization is characterized by TNF-α hypersecretion from activated macrophages.

Activated CD4⁺ T cells polarize to the T4-c phenotype via il-1α/β hyperactivation and in response to metal ion toxicity in the cirrhotic liver

Next, we assessed the immunomodulatory characteristics of activated $CD4^+$ T cells in the cirrhotic group. Reclustering of T cells exhibited six distinct clusters (Fig. S3A). We identified four major T-cell subtypes, including activated $CD4^+$ T cells, $CD8^+$ T cells, γδ T cells, and regulatory T cells (Tregs), in the cirrhotic group (Fig. 5A). Among them, $CD4^+$ T cells were significantly more abundant than other subtypes in cirrhosis when normalized to controls, prompting a focused analysis on this subset (Fig. 5B and S3B). These clusters were annotated into four distinct activated $CD4^+$ T-cell subtypes.

$CD4^+$ T cells from Cluster 3 were positioned at the root of the trajectory (pseudotime = 0), while $CD4^+$ T cells from Cluster 2 were located at the terminal end (Fig. 5C–D and S3C). Two major branch points were identified, segmenting the trajectory into five distinct cellular states (Fig. S3D), with State 4 being significantly more prevalent in cirrhotic samples (Fig. S3E). $CD4^+$ T cells from Cluster 4 exhibited enhanced differentiation within State 4 relative to the other states (Fig. S3F).

Despite limited overall intergroup differences in the pseudotime distribution, we focused on the second major branch point to further explore the functional divergences among the resulting lineages. Functional enrichment analyses of gene expression in the three branches revealed the following situations: cells in the prebranch (State 1; Cluster 4) were enriched in the "cellular response to metal ion" pathway; Branch 2 (State 4; Clusters 2 and 3) was associated with "MHC class Il protein complex binding", "MHC protein complex binding", "deoxycytidine deaminase activity" and "cytokine receptor activity"; and Branch 1 (State 3; Clusters 1 and 5) showed enrichment in the "leukocyte cell–cell adhesion", "regulation of cell–cell adhesion", "cytosolic ribosome" and "cytosolic small ribosomal" pathways (Fig. 5E and Table S6).

We subsequently conducted differential gene expression analysis on the activated $CD4^+$ T-cell populations from the cirrhotic and noncirrhotic groups and identified 221 significantly altered DEGs ($|\log 2FC| > 0.25$, $p < 0.05$; Table S7). The top 10 DEGs were visualized via bubble and heatmap plots, highlighting their distinct expression patterns (Fig. 5F and S3G). To elucidate the biological functions (BFs) of these DEGs in the activated $CD4^+$ T-cell populations, we performed enrichment analyses for GO terms (Table S8) and associated KEGG pathways (Table S9). The enriched GO terms among the DEGs included processes such as detoxification and stress responses to copper and cadmium ions (BP), localization to the MHC class II protein complex and endoplasmic reticulum lumen (CC), and functions such as MHC protein complex binding and transcription factor binding (MF) (Fig. S3H). KEGG pathway enrichment revealed involvement of the adherens junction and focal adhesion (cellular processes, CP), Wnt and VEGF signaling pathways (environmental information processing, EIP), and immune-related conditions such as viral myocarditis, allograft rejection (human diseases, HD), Th1/Th2 differentiation, and antigen processing and presentation (organismal systems, OS) (Fig. S3I).

To further characterize activated $CD4^+$ T-cell phenotypes in cirrhosis, we performed IREA on upregulated genes. The $CD4^+$ T-cell polarization radar plot indicated predominant T4-c polarization in cirrhotic samples. Consistently, cytokine enrichment analysis revealed strong enrichment of IL-1α and IL-1β in those $CD4^+$

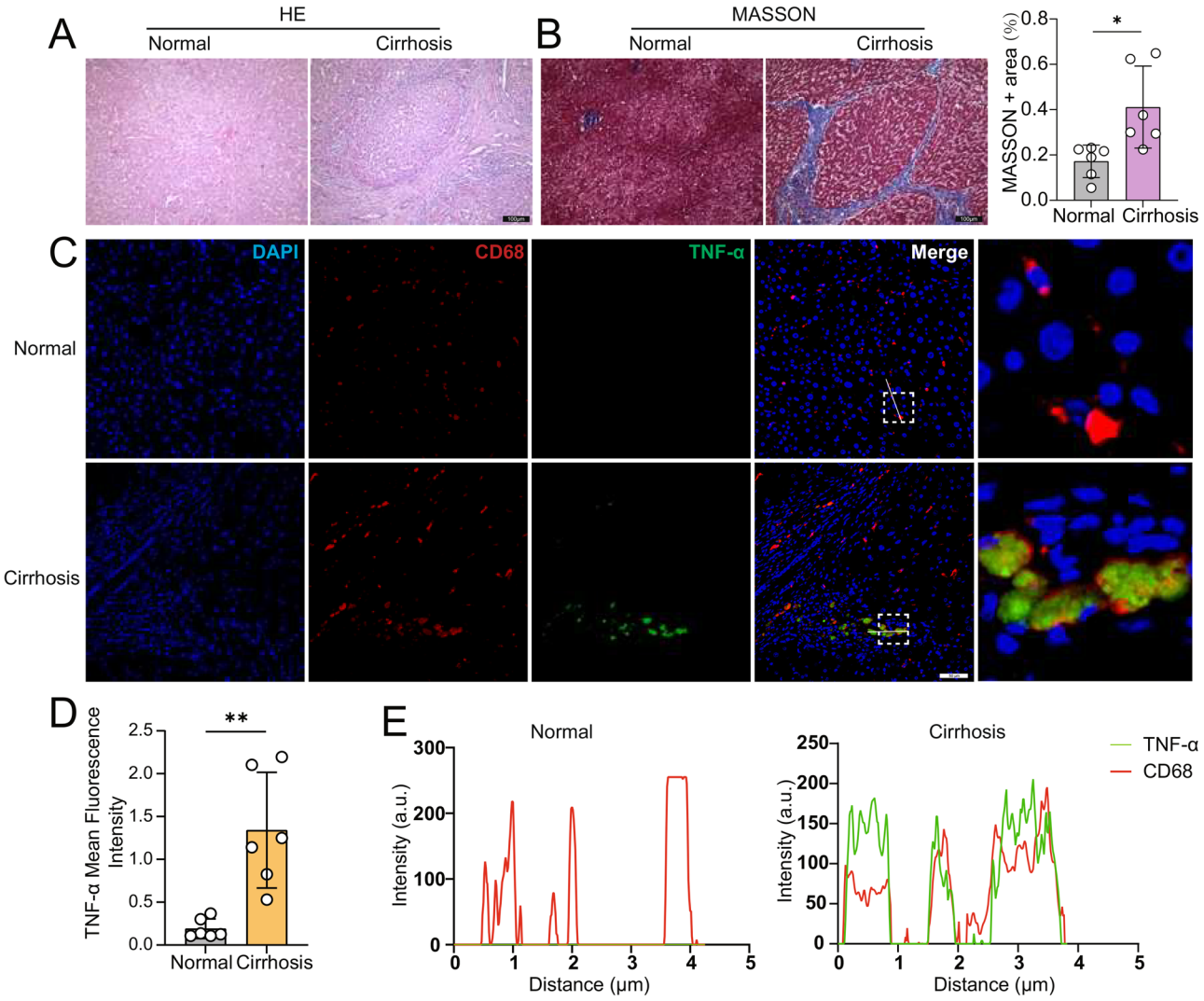

Fig. 4 Macrophage polarization toward TNF-α in liver cirrhosis progression. **A**) Representative H&E-stained histological liver sections with H&E. (scale bar = 100 μm). **B**) Representative histological liver sections Masson's trichrome. (scale bar = 100 μm). Positive areas were quantitatively analyzed ($n = 6$ per group). **C**) Representative immunofluorescence images of CD68 (red) and TNF-α (green) staining in liver sections. Nuclei were counterstained with DAPI (blue). (scale bar = 50 μm). **D**) The expression of TNF-α in the main liver tissue. The mean fluorescence intensity was calculated according to the following formula:integrated density (Intden)/total field area. **E**) Pearson correlation coefficient curves for colocalization analysis of CD68 and TNF-α in liver tissues. The results were analyzed via one-way ANOVA. Bars = means ± SDs. *$p < 0.05$, **$p < 0.01$, ***$p < 0.001$ and ns, not statistically significant

T-cell populations (Fig. 5G–H). Together, these findings suggest that cirrhotic liver-derived activated $CD4^+$ T cells exhibit a T4-c polarization profile (IL-1-driven effector/Th bias), as evidenced by IL-1α and IL-1β hyperactivation and a pronounced response to metal ion toxicity in the liver.

IFN-α/β enrichment induces NK cell polarization to the NK-a phenotype in cirrhosis.

To characterize NK cell polarization in cirrhosis, we conducted a detailed annotation of this cell population. Reclustering of NK cells yielded four distinct clusters via 13 PCs at a resolution of 0.2 (Fig. S4A, Fig. S5A).

The pseudotime trajectory analysis of NK cells from Cluster 3, located at the start of the trajectory (pseudotime = 0), revealed the earliest differentiation state, whereas the NK cells from Cluster 2 occupied the terminal end (Fig. S4B and S5B). A primary branch point along the trajectory resulted in the emergence of three distinct cellular states (Fig. S4C and S5C). We subsequently observed group-specific differentiation patterns. However, no significant differences were detected between State 2 and State 3 in either the cirrhotic or noncirrhotic samples (Fig. S5D). State 3 was notably more prevalent in the cirrhosis group. NK cells from Cluster 1 were predominantly enriched in State 3, indicating substantial differentiation in this subgroup (Fig. S5E). The functional

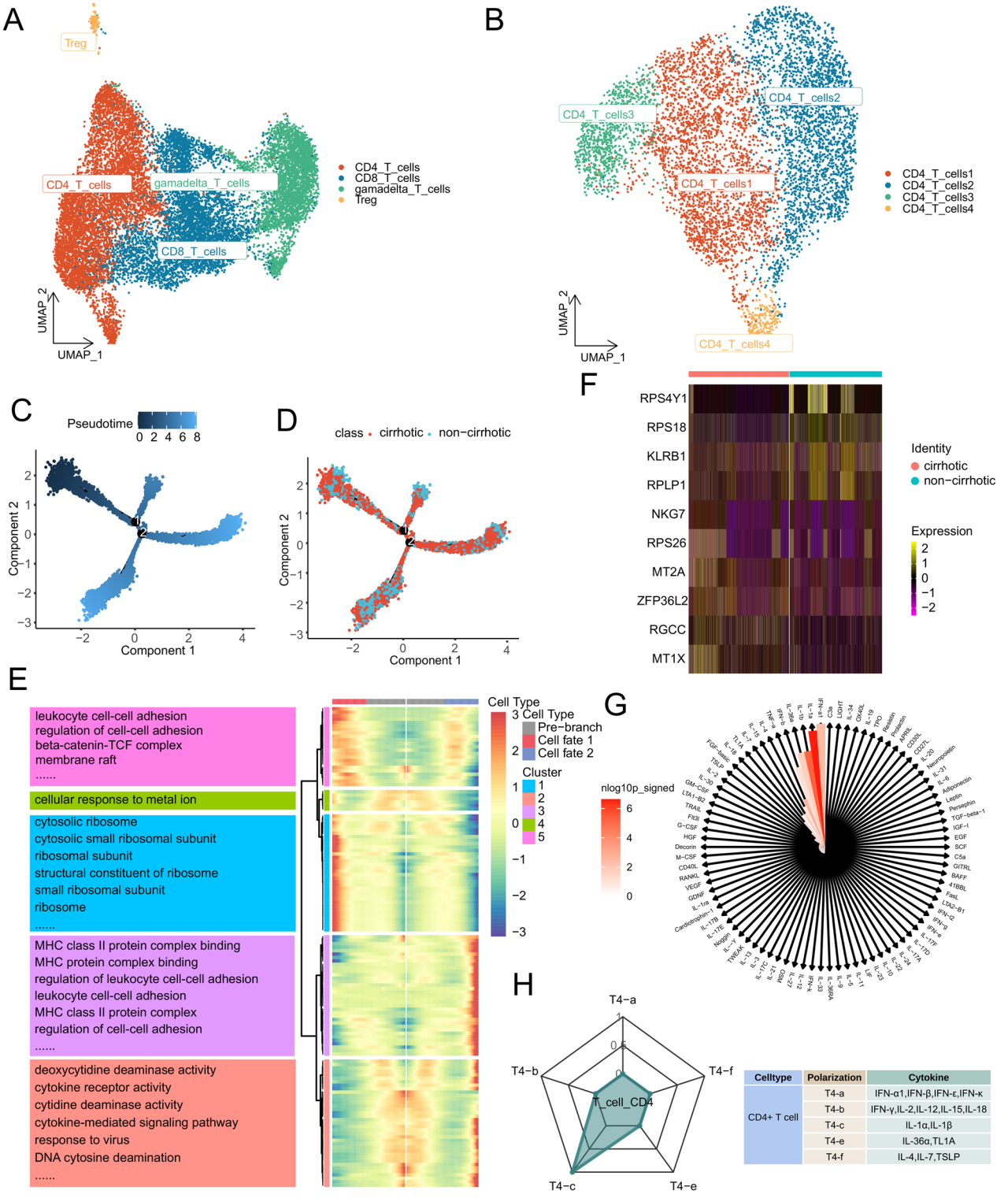

Celltype	Polarization	Cytokine
CD4+ T cell	T4-a	IFN-α1,IFN-β,IFN-ε,IFN-κ
	T4-b	IFN-γ,IL-2,IL-12,IL-15,IL-18
	T4-c	IL-1α,IL-1β
	T4-e	IL-36α,TL1A
	T4-f	IL-4,IL-7,TSLP

Fig. 5 T-cell reclustering, pseudotime trajectory reconstruction, and functional enrichment profiling. **A**) UMAP showed the annotation results of T-cell subgroups. **B**) UMAP presents the annotation results of $CD4^+$ T-cell subgroups. **C**) Pseudotime color transition from dark blue to light blue. **D**) Distribution of groups on the pseudotime trajectory. **E**) Heatmap illustrating the DEGs of various branches (cell fates). Enriched GO pathways of different gene clusters are shown on the left side of the heatmap. **F**) Heatmap displaying significant differential expression of 10 genes in $CD4^+$ T cells between the cirrhotic and noncirrhotic groups. **G**) Cytokine enrichment plot for $CD4^+$ T cells in cirrhosis. **H**) Radar plot and immune checkpoint card depicting cell polarization of $CD4^+$ T cells in cirrhosis

characterization of the three branches revealed distinct pathway enrichment: genes highly expressed in the prebranch (State 1, Cluster 2) were enriched in the "T-cell activation" pathway; genes in Branch 2 (State 3, Cluster 3) were associated with "regulation of hematopoiesis"; and those in Branch 1 (State 2, Cluster 1) were enriched in genes involved in "cell killing" (Fig. S4D and Table S10).

Next, we conducted differential expression analysis of NK cells from the cirrhotic and noncirrhotic groups and identified 325 significantly altered DEGs (|log2FC| > 0.25, $p < 0.05$; Table S11). The top 10 DEGs in NK cells were visualized via bubble and heatmap plots to highlight their expression trends (Fig. S4E and S5F). To elucidate the BF of these DEGs in NK cells, we performed GO (Table S12) and KEGG (Table S13) enrichment analyses. The GO analysis revealed enrichment of these genes in BPs such as "response to virus", "positive regulation of cytokine production", and "regulation of response to biotic stimulus"; enriched CCs included the "external side of plasma membrane" and "phagocytic vesicle"; and enriched MFs included "thioesterase binding" and "serine/threonine phosphatase activity" (Fig. S5G).

KEGG pathway analysis revealed that the DEGs were involved in diverse CPs, including "phagosome," "endocytosis," and "cellular senescence." Additionally, pathways related to immune regulation and infection, such as "cell adhesion molecules (EIP)," "NK cell-mediated cytotoxicity," "Fc gamma R-mediated phagocytosis," and "leukocyte transendothelial migration" in OS, were significantly enriched. Viral disease-related pathways, including "HIV-1 infection (Genetic Information Processing, GIP)," "human cytomegalovirus infection," and "Kaposi sarcoma-associated herpesvirus infection" in HD, were also prominent (Fig. S5H). To assess the functional polarization of NK cells, we performed IREA on genes significantly upregulated in cirrhotic NK cells. The NK cell polarization radar chart indicated a dominant NK-a polarization phenotype (type I IFN-responsive cytotoxic) in cirrhosis (Fig. S4F). Furthermore, cytokine enrichment analysis revealed increased expression of IFN-α1 and IFN-β in cirrhosis-associated NK cells (Fig. S4G).

EGF expression polarizes B cells to the B-e phenotype in cirrhosis

We classified the population into three unique B-cell subtypes (Fig. S6A, Fig. S7A). To explore the functional heterogeneity of these B cells during differentiation, we established a pseudotime trajectory of cellular differentiation (Fig. S6B and S7B).Two major branch points were identified along the differentiation trajectory, resulting in five distinct cellular states (Fig. S6C and S7C). The differential distribution of these states revealed notable differences between the cirrhotic and noncirrhotic groups, particularly in State 1, which was significantly enriched in cirrhosis samples (Fig. S7D-E). Notably, B cells from Cluster 2 predominantly contributed to this state (Fig. S7E). Given the limited overall differences in pseudotime trajectories between the two groups, we focused on branch point 1 for further functional analysis. Enrichment analysis of genes associated with each branch revealed distinct pathway involvement, such as genes in the prebranch (State 4, Cluster 3), which were enriched primarily in "regulation of hematopoiesis". Branch 2 (State 5, Cluster 1) was enriched in "positive regulation of lymphocyte activation", whereas Branch 1 (State 1, Cluster 2) was characterized by genes involved in the "regulation of response to osmotic stress" (Fig. S6D and Table S14).

Subsequent differential expression analysis of activated B-cell subpopulations from the cirrhotic and noncirrhotic groups revealed 383 significantly altered DEGs (|log2FC| > 0.25, $p < 0.05$, Table S15). Bubble and heatmap plots highlighted the top 10 DEGs and their expression profiles in B cells (Fig. S6E and S7F). To investigate the BF of these DEGs in B cells, enrichment analyses were performed for GO terms (Table S15) and KEGG pathways (Table S17). The GO analysis revealed enrichment of these genes in processes such as "cytoplasmic translation", "B-cell activation", and "regulation of B-cell activation" (BP); components including "cytosolic ribosome", "focal adhesion", and "cell-substrate junction" (CC); and functions such as "structural constituent of ribosome", "rRNA binding", and "immunoglobulin receptor binding" (MF) (Fig. S7G). The KEGG pathway enrichment further revealed significant involvement in "regulation of actin cytoskeleton" (CP), "ribosome" (GIP), "Salmonella infection", "viral myocarditis" (HD), "hematopoietic cell lineage", "intestinal immune network for IgA production", and "mineral absorption" (OS) (Fig. S7H).

Finally, IREA of genes upregulated in cirrhotic B cells revealed a dominant B-e polarization profile, with the expression of the cytokines CD40L and IL-21. The polarization radar plot revealed a B-e phenotypic bias (EGF-enriched B phenotype) in cirrhotic samples, and cytokine enrichment analysis revealed elevated expression of EGF (Fig. S6F-G). These findings suggest that activated B cells in cirrhosis undergo pseudotime-restricted differentiation, biased toward State 1 (B cells enriched in Cluster 2). This reprogramming is characterized by increased ribosome-mediated cytoplasmic translation and EGF hypersecretion, indicative of a B-e polarization phenotype.

IL-1β polarizes monocytes to the Mono-c phenotype in cirrhosis

The monocyte populations were reclustered at a resolution of 0.2 using 11 PCs, resulting in five distinct clusters (Fig. S9A). These genes were further annotated into five unique monocyte subtypes (Fig. S8A and S9B). To

explore functional heterogeneity during differentiation, we constructed a pseudotime trajectory for monocytes (Fig. S8B-C). Four major branch points were identified along the entire trajectory, resulting in nine distinct cellular states (Fig. S9C). Analysis of group-specific differentiation patterns revealed significant differences in State 2 between the cirrhotic and noncirrhotic groups (Fig. S9D-E). Monocytes from Cluster 2 displayed substantial differentiation in State 2.

Enrichment analysis of genes associated with each resulting branch revealed the following: prebranch cells (State 1, Cluster 4) were enriched in the "MHC class II protein complex assembly" pathway; Branch 2 (State 3, Clusters 1 and 3) was associated with the "defense response to fungus"; and Branch 1 (State 2, Cluster 2) was enriched in "leukocyte tethering or rolling" (Fig. S8D and Table S18).

Differential gene expression analysis of monocytes from the cirrhotic and noncirrhotic groups revealed 426 significantly altered DEGs ($|\log2FC| > 0.25$, $p < 0.05$; Table S19). The top 10 DEGs were visualized via bubble plots and heatmaps to illustrate their expression profiles (Fig. S8E and S9F). To investigate the BF of these DEGs in monocytes, we performed enrichment analysis for GO terms (Table S20) and KEGG pathways (Table S21). GO terms revealed enrichment in BPs such as "cytoplasmic translation," "B-cell activation," and "regulation of B-cell activation"; CCs included "cytosolic ribosome," "focal adhesion," and "cell-substrate junction"; and MFs included "structural constituent of ribosome," "rRNA binding," and "immunoglobulin receptor binding" (Fig. S9G). KEGG pathway analysis revealed enrichment in processes such as "regulation of the actin cytoskeleton," "ribosome," and various immune- and infection-related pathways such as "Salmonella infection," "viral myocarditis," "hematopoietic cell lineage," and the "intestinal immune network for IgA production" (Fig. S9H). The polarization radar chart revealed that monocytes in the cirrhosis group predominantly exhibited a Mono-c polarization state (IL-1-skewed antigen presentation). Cytokine enrichment analysis also revealed strong enrichment of the cytokines IL-1α, IL-1β, and IL-36α in cirrhotic monocytes (Fig. S8F-G).

SCENIC analysis revealed cell subtype-specific transcription factor dynamics underlying immune dysregulation in patients with liver cirrhosis

In macrophages, bubble plot analysis revealed notable differences in TF activity between the cirrhotic and noncirrhotic groups (Fig. 6A). UMAP visualization further demonstrated that these TFs were predominantly expressed in the Macrophage_3 subtype (Fig. 6B). Similarly, significant differences in the expression of potential TFs were observed via bubble plots and corresponding UMAP analyses of T cells (Fig. 6C–D), NK cells (Fig. 6E–F), B cells (Fig. 6G–H), and monocytes (Fig. 6I–J) between the cirrhotic and noncirrhotic groups. Moreover, UMAP analysis revealed that these TFs were highly expressed in specific subpopulations of immune cells, such as $CD4^+$ T-cell subgroups (Fig. 6D), NK cells from Cluster 2 (Fig. 6F), and monocytes from Cluster 3 (Fig. 6J). Collectively, these findings suggest the dynamic regulatory landscape of immune cell subtypes in liver cirrhosis and provide valuable insights into the transcriptional reprogramming that drives immune dysregulation during disease progression.

SCENIC analysis reveals cytokine networks driving immune dysregulation in cirrhosis

Using SCENIC analysis, we identified TFs that were significantly expressed across various immune cell subtypes in cirrhotic samples. We then systematically integrated these TFs with their associated cytokines secreted by each immune cell type, and the results are summarized in Table 1. To illustrate cytokine distribution, we generated a pie chart based on the cytokine frequency (Fig. 7A). Notably, IFN-β1 was highly expressed in $CD4^+$ T cells from cirrhotic liver samples and in monocytes from noncirrhotic samples (Fig. 7B); IL-1β showed high expression in monocytes under both cirrhotic and noncirrhotic conditions (Fig. 7C, D).A corresponding UMAP visualization of TF expression revealed that thyroid hormone receptor alpha (THR-α) was highly expressed in $CD4^+$ T cells derived from cirrhotic samples but was more prominent in SMCs from noncirrhotic liver samples (Fig. 7E). Additionally, ETS proto-oncogene 2, a transcription factor (*ETS2*), was predominantly expressed in macrophages in cirrhotic livers, whereas it was more highly expressed in endothelial cells in noncirrhotic samples (Fig. 7F). Overall, these transcription factor regulon networks delineate the transcriptional regulatory landscape across various cell lineages within the cirrhotic immune microenvironment, revealing pivotal regulatory axes that drive immune reprogramming during cirrhosis progression.

Fibroblast-mediated macrophage migration inhibitory factor (MIF) signaling is activated in cirrhosis

We investigated intercellular communication across all cell types and identified fibroblasts as key mediators, displaying substantial alterations in signaling interactions between cirrhotic and noncirrhotic conditions. Quantitative analysis revealed a significant enhancement in overall signaling activity in cirrhosis: the total interaction count increased from approximately 10,075 in noncirrhotic controls to 11,436 in cirrhotic samples, with an average communication strength elevated by approximately 1.5-fold (permutation test, $p = 0.018$) (Fig. 8A). Network analysis revealed that fibroblast-mediated

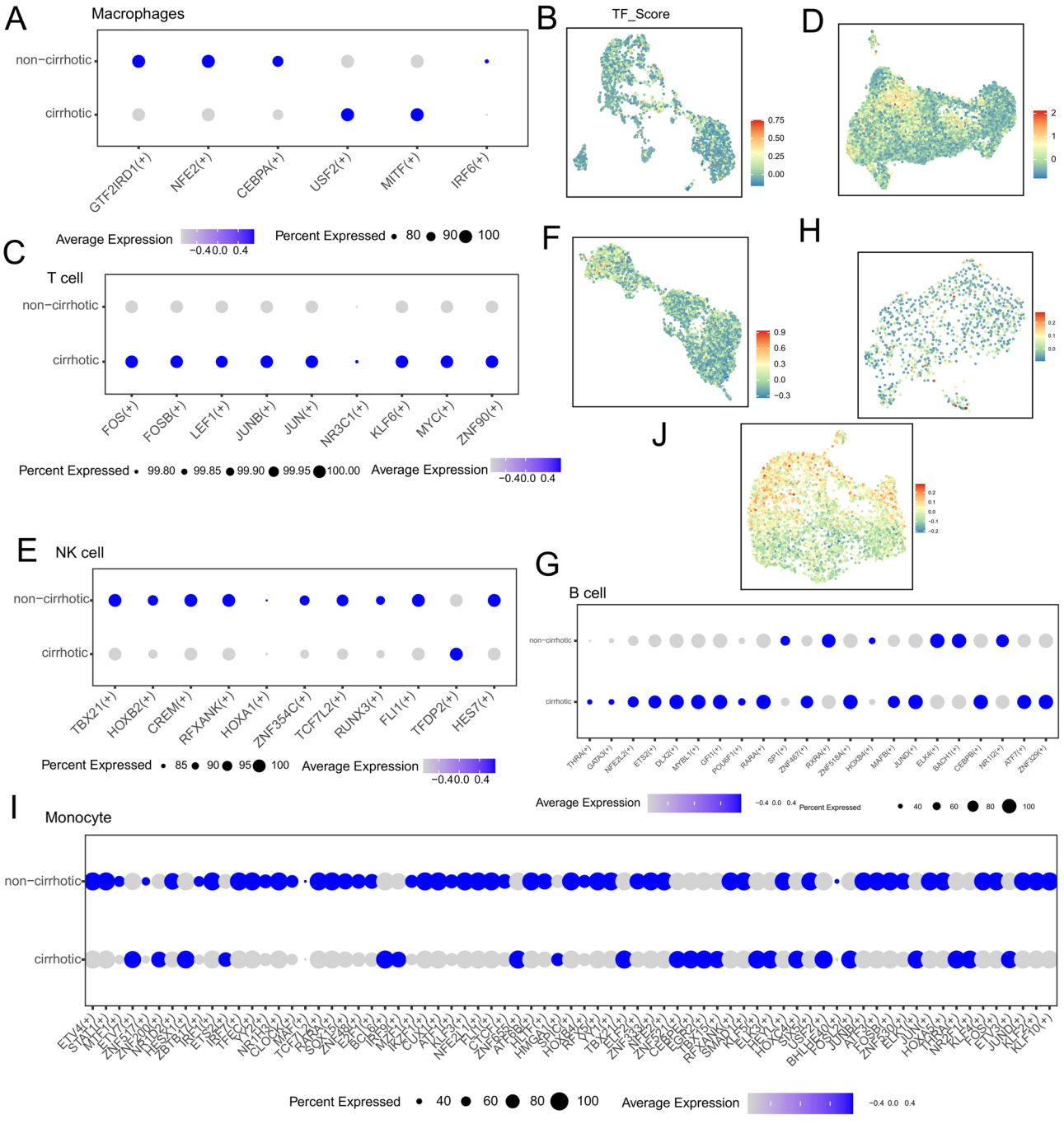

Fig. 6 Transcription factor analysis of macrophages, T cells, NK cells, B cells, and monocytes in cirrhotic liver samples. **A**) Bubble plots displaying the distribution of transcription factor expression in macrophages across different groups. **B**) The UMAP plot shows the clustering of TFs in macrophage subgroups. **C**) Bubble plots demonstrating the distribution of TFs in T cells among different groups. **D**) The UMAP plot displays the clustering of TFs in T-cell subgroups. **E**) Bubble plots show the distribution of TFs in NK cells across different groups. **F**) The UMAP plot exhibits the clustering of TFs in NK cell subgroups. **G**) The bubble plot indicates the distribution of transcription factor expression in B cells across different groups. **H**) The UMAP plot shows the transcription factor clusters in B-cell subgroups. **I**) The bubble plot demonstrates the distribution of TFs in monocytes across different groups. **J**) The UMAP plot illustrates the transcription factor clusters in the monocytic subgroups

signaling was significantly elevated in cirrhosis patients in terms of both frequency and strength (Fig. 8B). Further comparison of global signaling patterns between these two groups revealed distinct shifts in intercellular communication networks (Fig. 8C).

The MIF signaling pathway has emerged as a key regulatory axis that is specifically amplified in cirrhosis. Under cirrhotic conditions, fibroblasts significantly upregulated the expression of MIF and its homolog D-DT ligands ($\log_2 FC \approx 1.2$, $p < 0.01$). These ligands showed

Table 1 Summary of cell factors and transcription factors

Celltype	Cytokine(s)	TF(s)
Macrophage_3	TNF–α, IL–1α, IL–15, IL–1b, IFN–γ	USF2(+), MITF(+)
$CD4^+$ T	IFN–α1, IL–1α, IL–36α, IL–1β, IFN–β	FOS(+), FOSB(+), LEF1(+), JUNB(+), JUN(+)
NK cells	IFN–α1, IL–15, IFN–β, IL–18, IL–12	TFDP2(+)
B cells	IL–4, IFN–α1, IFN–β, IL–21, EGF	THRA(+), GATA3(+), NFE2L2(+), ETS2(+), DLX2(+)
Monocytes	IL–1β, IL–36α, GM–CSF, TNF–α, IFN–α1	ETV7(+), ZNF200(+), HESX1(+), ETS2(+), BCL6(+)

increased interaction with their corresponding receptors (CD74, CXCR4, and CD44) on B cells, the expression of which was also markedly increased (Cohen's d ≈ 0.8) (Fig. 8D). Violin plots further confirmed the upregulation of MIF ligands and receptors across cell types, with a notable increase in MIF receptor expression in B cells from cirrhotic livers (Fig. 8E). This coordinated upregulation supports the establishment of a strengthened MIF signaling axis between fibroblasts and B cells. Downstream, the expression of signaling genes such as *JUN*, and *IL1B* was synchronously elevated, indicating the activation of MIF-mediated signaling cascades. Statistical analysis via permutation tests confirmed that MIF signaling from

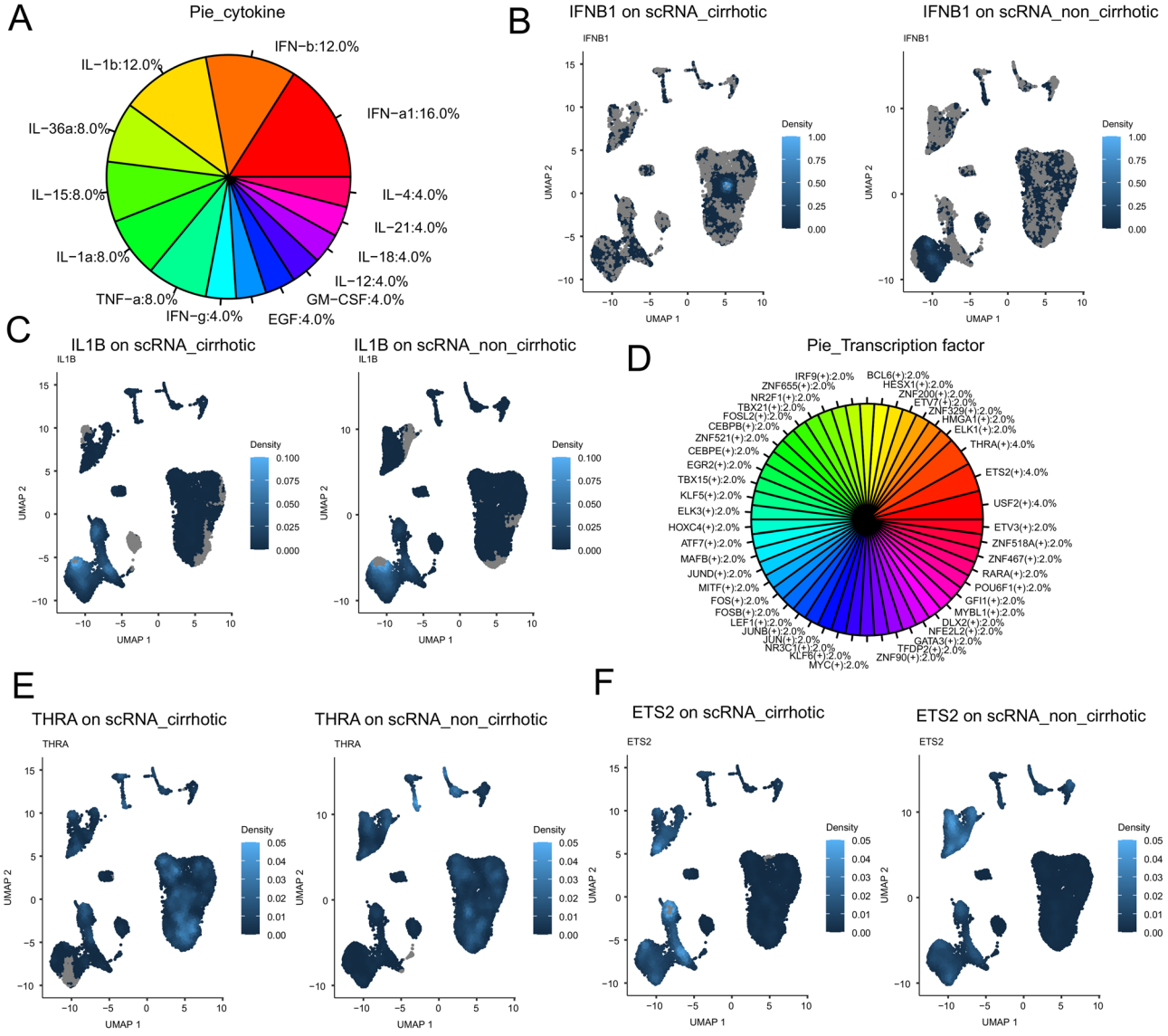

Fig. 7 Summary of cytokines and their respective expression in all cell types under cirrhotic and noncirrhotic conditions. **A**) Pie chart showing the frequency of cytokines. **B**) UMAP plot depicting the expression of the cytokine IFN-β1 in cirrhotic and noncirrhotic states. **C**) The UMAP plot illustrates the expression of the cytokine IL-1β under cirrhotic and noncirrhotic conditions. **D**) Pie chart showing transcription factor frequencies. **E**) UMAP plot of the transcription factor THR-α in cirrhotic and noncirrhotic livers. **F**) UMAP plot of ETS2 in cirrhotic and noncirrhotic livers

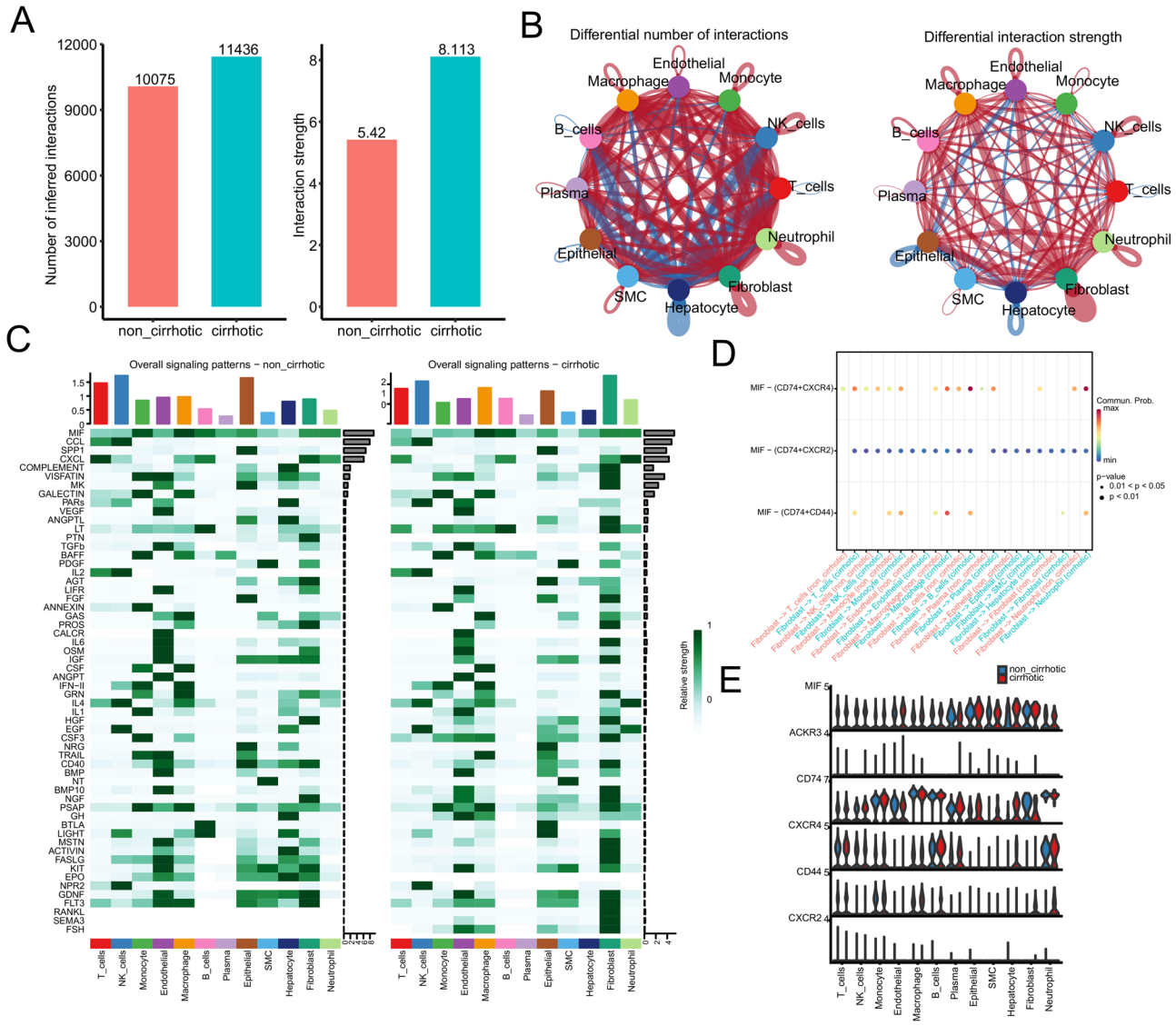

Fig. 8 The overall patterns of cell communication between the cirrhotic and noncirrhotic groups. **A**) Bar graphs depict the total number and strength of interactions among all cell types in single cells from cirrhotic and noncirrhotic groups. **B**) Network graphs demonstrate intergroup variations in the number and strength of interactions among different cell types in the cirrhotic and noncirrhotic groups, with red lines indicating an increase in communication quantity and intensity in cirrhotic compared to noncirrhotic groups, and blue lines indicating a decrease. Left: communication quantity, right: communication intensity. **C**) Heatmaps illustrate the signaling pathways contributing most significantly to overall cell communication in the cirrhotic versus noncirrhotic groups. **D**) Enhanced receptor profiles mediating communications between fibroblasts and other cell types in the cirrhotic group. **E**) Violin plots show the expression distributions of MIF signaling receptors in the cirrhotic versus noncirrhotic groups

fibroblasts to B cells was significantly increased in cirrhosis patients ($p < 0.05$), with a large effect size (Cohen's $d > 0.8$) (Table S22-23). To further validate the expression patterns of MIF, B cells, and their corresponding receptors in cirrhotic livers, we performed histological staining on liver sections from clinical cirrhosis patients and controls. HE and Masson staining revealed markedly increased collagen deposition in the cirrhotic group (Fig. 9A, B). Immunofluorescence analysis revealed substantial upregulation of MIF expression in cirrhotic tissues, which clearly colocalized with the B-cell marker CD19 and the MIF receptor CXCR4 (Fig. 9 C-E). These morphological findings provide tangible support for the enhanced MIF signaling axis between fibroblasts and B cells within the cirrhotic microenvironment. Collectively, these findings suggest that fibroblast-derived MIF signaling is a pivotal pathway activated in cirrhosis and likely plays a key role in remodeling the immune microenvironment.

Discussion

This study utilized an integrated single-cell analytical framework to investigate the dynamic changes and functional reprogramming of immune cells in liver cirrhosis. The analysis revealed lineage-specific transformation

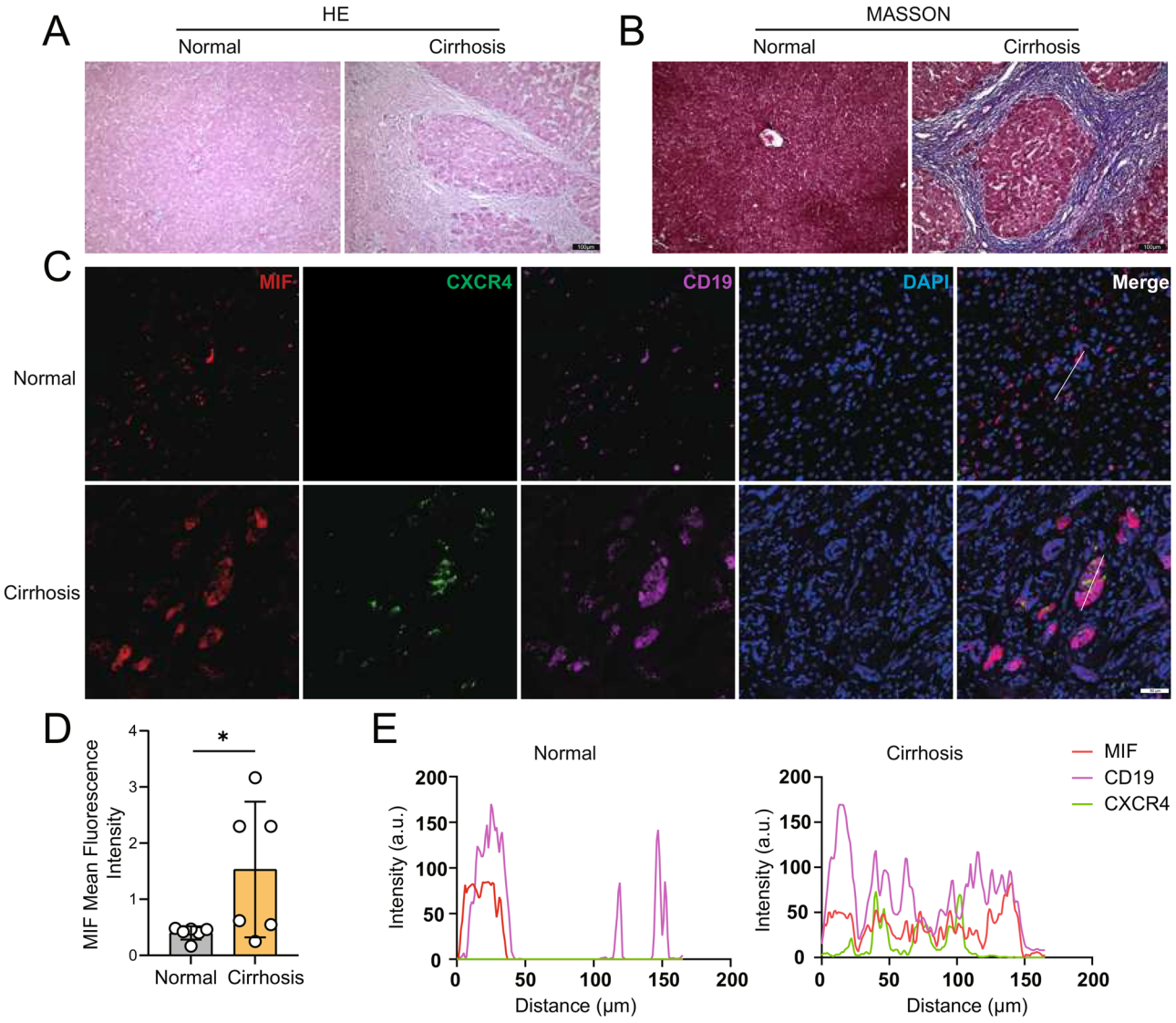

Fig. 9 The MIF-CXCR4–CD19 regulatory axis is activated during liver cirrhosis progression. **A**) Representative H&E-stained histological liver sections. (scale bar = 100 μm). **B**) Representative histological liver sections subjected to Masson's trichrome staining. (scale bar = 100 μm). The positive areas were quantitatively analyzed ($n = 6$ per group). **C**) Representative immunofluorescence images of CD19 (purple), MIF (red) and CXCR4 (green) staining in liver sections. Nuclei were counterstained with DAPI (blue). (scale bar = 50 μm). **D**) The expression of MIF in the main liver tissue. The mean fluorescence intensity was calculated according to the following formula: integrated density (Intden)/total field area. **E**) Pearson correlation coefficient curves for colocalization analysis of CD19, MIF and CXCR4 in liver tissues. The results were analyzed via one-way ANOVA. Bars = means ± SDs. *$p < 0.05$, **$p < 0.01$, ***$p < 0.001$ and ns, not statistically significant

pathways, highlighting three key axes influencing disease-related immune regulation: TNF-α/*ETS2*-driven polarization of macrophages toward a Mac-d phenotype, IL-1α/β/*THRA*-associated polarization of $CD4^+$ T cells toward a T4-c phenotype, and enhancement of the fibroblast-to-B-cell MIF signaling axis. These findings offer potential avenues for understanding the immune mechanisms of cirrhosis and devising targeted interventions.

Within the macrophage compartment, the Macrophage_3 subpopulation was enriched in late pseudotime, indicating a terminally differentiated state. IREA profiling confirmed its Mac-d polarized signature, accompanied by elevated TNF-α expression. Transcriptional regulatory analysis revealed increased ETS2 activity in this subpopulation, potentially cooperating with TNF-α signaling to increase inflammation, highlighting the pivotal role of the TNF-α/*ETS2* axis in promoting chronic inflammation in patients with cirrhosis. Elevated TNF-α levels in the livers of patients with cirrhosis are positively correlated with disease severity [34]. TNF-α activates the NF-κB and MAPK pathways, leading to hepatocyte apoptosis and hepatic stellate cell activation, thereby promoting fibrosis [35]. TNF-α amplifies the inflammatory response by regulating IL-6 and IL-1β and directly induces hepatic

stellate cell transdifferentiation, exacerbating liver fibrosis [36, 37].

$CD4^+$ T cells are notably expanded in cirrhosis patients and are predominantly found in State 4 of the pseudotemporal trajectory, a branch linked to metal ion stress and antigen presentation functions. Analysis via IREA revealed a significant increase in IL-1α and IL-1β expression, characterizing a T4-c-polarized phenotype. Integration with regulatory network data revealed that *THRA* was coactivated in this cell population, potentially playing a role in regulating IL-1-responsive genes. These findings collectively suggest that the IL-1α/β–*THRA* axis-driven T4-c polarization of $CD4^+$ T cells contributes to inflammatory amplification in the immune microenvironment of cirrhosis. IL-1β stimulates Kupffer cell activation and induces HSC proliferation and activation through the NLRP3 inflammasome-CASP1 signaling pathway, exacerbating hepatic fibrosis. In animal models of liver fibrosis, IL-1β inhibitors such as anakinra have shown substantial potential in reducing inflammation and fibrosis [38–40]. These findings highlight IL-1β as a central mediator of inflammatory responses in cirrhosis and underscore its promise as a therapeutic target for early intervention.

The enrichment analyses revealed significant alterations in the cellular signaling and metabolic pathways associated with immune cells in patients with liver cirrhosis. Specifically, the identified pathways, such as endocytosis, phagosomes, and antigen processing and presentation, highlight the critical role of immune cell function in the pathogenesis of liver cirrhosis [38, 41, 42]. These pathways are essential for the immune response, as they facilitate the uptake and processing of antigens, which is crucial for effective immune surveillance and response to liver injury. The enrichment of genes involved in "cytoplasmic translation" and "ribosome biogenesis" suggests that under conditions of liver cirrhosis, immune cells may undergo significant metabolic reprogramming and protein translation activation to support their immune response in the inflammatory microenvironment and the demands of cytokine secretion. This finding is consistent with the persistent immune activation state in cirrhosis [43]. Notably, enrichment of the "cytoplasmic translation" and "ribosome biogenesis" pathways was consistently observed in all immune subsets, indicating a systematic signaling pattern that likely reflects the authentic physiological state of immune cells in the cirrhotic microenvironment. Future studies will involve sensitivity analyses, such as including the ribosomal protein-encoding gene (RPG) proportion as a covariate in normalization or differential expression analysis or conducting enrichment and clustering analyses after excluding RPGs, to confirm the robustness of our core biological findings.

ETS2 is an ETS-family transcription factor and proto-oncogene [44]. In a liver fibrosis model, macrophages lacking *ETS2* presented a 3–5-fold increase in IL-1β expression when stimulated with HMGB1 or LPS, while overexpression of *ETS2* significantly reduced the levels of IL-1β, IL-6, and other inflammatory factors and suppressed *TLR4*-NF-κB pathway activation, thereby alleviating hepatocyte necrosis and periportal fibrosis [45]. Contrary to the protective role of *ETS2*, *USF2* promotes the release of inflammatory factors, such as IL-1β, through multiple pathways, driving the progression of liver fibrosis. Experimental evidence indicates that *USF2* transcriptionally activates THBS1, subsequently activating the TGF-β/Smad3/NLRP3/Caspase-1 pathway and leading to increased expression of IL-1β and IL-18 [46]. The two exhibit antagonistic regulation within macrophages, forming a crucial balance axis in the inflammatory–fibrotic response in cirrhosis.

The study also revealed a notable increase in both the frequency and intensity of communication between fibroblasts and B cells within cirrhotic tissue. The MIF ligand–receptor pathway has emerged as a pivotal signaling axis, with fibroblasts releasing MIF ligands and B cells showing increased expression of the receptors CD74 and CXCR4. IREA findings indicated polarization toward a B-e state in B cells, concomitant with elevated levels of EGF and IL-21. This increase in fibroblast-B-cell MIF signaling is likely to aggravate the progression of cirrhosis through proinflammatory and profibrogenic mechanisms. These findings are consistent with and extend previous clinical observations. Previous studies have shown that MIF levels are significantly elevated in sera from patients with HCC and liver cirrhosis compared with those from patients with gastrointestinal cancer and normal controls [47]. The balance between MIF and sCD74 is predictive of outcomes in individuals experiencing acute decompensation of cirrhosis [48]. The identification of these genes and their altered expression patterns underscore their potential as therapeutic targets and biomarkers for monitoring disease progression and treatment efficacy in patients with liver cirrhosis.

The dataset utilized in this investigation comprises 5 cirrhotic and 7 control samples. Although the utilization of a single-center sequencing platform ensures data consistency, the limited sample size may exacerbate the influence of interindividual biological variability on the analysis of immune cell subsets. The dataset's high sequencing depth and coverage, however, offer a strong framework for exploring immune diversity. To harmonize the data and address potential batch effects (e.g., stemming from library preparation and sequencing runs), we employed the Harmony algorithm, a commonly utilized tool for integrating single-cell data across multiple samples [49, 50]. Harmony mitigates technical variations by

aligning shared feature spaces iteratively across samples. Following this correction, UMAP visualization revealed a homogeneous distribution of cells from various samples, with no discernible batch-specific clustering, indicating successful elimination of batch effects. This robust integration establishes a reliable foundation for subsequent comparative analysis of immune subpopulations.

This study acknowledges several limitations that warrant careful consideration. First, owing to the scarcity of scRNA-seq data of cirrhotic liver tissues in public databases, the relatively small sample size analyzed in this study might hinder the generalizability of the results, as it might not capture the full spectrum of cellular heterogeneity present in cirrhosis. Second, the lack of spatial transcriptomic information limits the understanding of the spatial localization and interactions among immune cell populations, impeding a comprehensive analysis of immune cell cooperativity. Third, the absence of detailed clinical and grouping metadata for each donor hindered donor-specific analyses, such as individual UMAP projections and abundance distribution analyses, leading to findings that primarily reflect population-level trends. To validate and expand upon our results, further research using large-scale, multicenter cohorts and multidimensional experimental approaches is needed. Future studies will incorporate spatial transcriptomics, high-dimensional multiomics, and functional analyses to increase the biological and translational significance of these findings.

Conclusions

In summary, immune cells in cirrhosis exhibit significant reprogramming characteristics, with the TNF-α/*ETS2*, IL-1α/β/*THRA*, and MIF signaling pathways forming a fundamental immunoregulatory network. This network offers valuable insights into the immune mechanisms involved in cirrhosis, suggesting promising targets for intervention.

Supplementary information

The online version contains supplementary material available at https://doi.org/10.1186/s12967-026-07858-z.

Supplementary Material 1

Supplementary Material 2

Supplementary Material 3

Supplementary Material 4

Supplementary Material 5

Supplementary Material 6

Supplementary Material 7

Supplementary Material 8

Supplementary Material 9

Supplementary Material 10

Supplementary Material 11

Acknowledgements
We sincerely thank Professor Jingfang Hong for her assistance.

Authors' contributions
Q. Z. and N. Z. analyzed the data. X-L.K. provided clinical samples and assisted in detection. Z-C. Z. and H.L. were involved in designing the experiments and analyzing the data. Y. F. performed the staining of patient liver tissues. Q. Z. and Y. C. wrote the manuscript and performed critical revisions of the article. All the authors have read and approved the submitted version.

Funding
The study was supported by the National Natural Science Foundation of China (82402657 to Y.C.) and the Natural Science Research Project of Higher Education in Anhui Province of China (2024AH050685 to Y.C.).

Data availability
ScRNA-seq data for cirrhosis patients were obtained from the Gene Expression Omnibus (GEO) database under accession number GSE168933. The data that support the findings of this study are available from the corresponding author upon reasonable request.

Declarations

Ethics approval and consent to participate
The single-cell RNA sequencing data used in this study were obtained from publicly available data in GEO databases and did not involve ethical approval or consent to participate. Liver tissue specimens were obtained from patients at the Second Affiliated Hospital of Anhui Medical University (Hefei, China) in compliance with the Declaration of Helsinki. The study protocol received approval from the Anhui Medical University Ethics Committee and the Second Hospital of Anhui Medical University Ethics Committee (permit numbers: 83242368 and YX2025–256). Prior to participation, written informed consent was obtained from all the subjects.

Consent for publication
All the authors provided consent for publication.

Competing interests
The authors declare no competing interests.

Author details
[1]School of Nursing, Anhui Medical University, Hefei 230032, China
[2]Department of Nursing, The Second Affiliated Hospital of Anhui Medical University, Hefei 230601, China
[3]Department of Biochemistry and Molecular Biology, Research Center for Infectious Diseases, School of Basic Medical Sciences, Anhui Medical University, Hefei 230032, China
[4]Department of Rehabilitation Medicine, The Second Affiliated Hospital of Anhui Medical University, Hefei 230032, China

Received: 6 September 2025 / Accepted: 6 February 2026
Published online: 17 February 2026

References

1. Xiao S, Xie W, Zhang Y, Lei L, Pan Y. Changing epidemiology of cirrhosis from 2010 to 2019: results from the global burden disease study 2019. Ann Med. 2023;55:2252326.
2. Maher JJ. Not the end of the road for macrophage therapy in liver cirrhosis. Nat Med. 2025;31:735–36.
3. Tapper EB, Goldberg D, Parikh ND, Terrault NA, Welch N, Sharpton S, Hameed B, Khalili M, Stolz A, Verna EC, et al. The liver cirrhosis network cohort study: cirrhosis definition, study population, and endpoints. Am J Gastroenterol. 2025;120:570–75.

4. Imbert-Bismut F, Ratziu V, Pieroni L, Charlotte F, Benhamou Y, Poynard T. Biochemical markers of liver fibrosis in patients with hepatitis C virus infection: a prospective study. Lancet. 2001;357:1069–75.
5. Zieve L. Jaundice in cirrhosis. Jama. 1965;191:475–79.
6. Thieu HV, Minh TB, Tuong TK. Duc NM: cutoff values for serum ferritin in predicting cirrhosis severity due to cholestatic jaundice in Vietnamese children. Med Arch. 2022;76:122–26.
7. Moore CM, Van Thiel DH. Cirrhotic ascites review: pathophysiology, diagnosis and management. World J Hepatol. 2013;5:251–63.
8. Moore KP, Aithal GP. Guidelines on the management of ascites in cirrhosis. Gut. 2006;55(Suppl, 6):vi1–12.
9. Romero-Gómez M, Montagnese S, Jalan R. Hepatic encephalopathy in patients with acute decompensation of cirrhosis and acute-on-chronic liver failure. J Hepatol. 2015;62:437–47.
10. Gilgenkrantz H, Sayegh RA, Lotersztajn S. Immunoregulation of liver fibrosis: new opportunities for antifibrotic therapy. Annu Rev Pharmacol Toxicol. 2025;65:281–99.
11. Fattovich G, Stroffolini T, Zagni I, Donato F. Hepatocellular carcinoma in cirrhosis: incidence and risk factors. Gastroenterology. 2004;127:S35–50.
12. Bengtsson B, Widman L, Wahlin S, Stål P, Björkström NK, Hagström H. The risk of hepatocellular carcinoma in cirrhosis differs by etiology, age and sex: a Swedish nationwide population-based cohort study. U Eur Gastroenterol J. 2022;10:465–76.
13. Lin J, Wu JF, Zhang Q, Zhang HW, Cao GW. Virus-related liver cirrhosis: molecular basis and therapeutic options. World J Gastroenterol. 2014;20:6457–69.
14. Morgan TR. Treatment of alcoholic liver disease. Gastroenterol Hepatol (N Y). 2017;13:425–27.
15. Seki E, Schwabe RF. Hepatic inflammation and fibrosis: functional links and key pathways. Hepatology. 2015;61:1066–79.
16. Koyama Y, Brenner DA. Liver inflammation and fibrosis. J Clin Invest. 2017;127:55–64.
17. Guilliams M, Scott CL. Liver macrophages in health and disease. Immunity. 2022;55:1515–29.
18. Feng X, Feng B, Zhou J, Yang J, Pan Q, Yu J, Shang D, Li L, Cao H. Mesenchymal stem cells alleviate mouse liver fibrosis by inhibiting pathogenic function of intrahepatic B cells. Hepatology. 2024.
19. Chen G, Xu W, Long Z, Chong Y, Lin B, Jie Y. Single-cell technologies provide novel insights into liver physiology and pathology. J Clin Transl Hepatol. 2024;12:79–90.
20. Liu W, Li M, Guo H, Wei S, Xu W, Yan Y, Shi Y, Xu Z, Chang K, Wei G, Zhao S. Single-cell transcriptome analysis of liver immune microenvironment changes induced by microplastics in mice with non-alcoholic fatty liver. Sci Total Environ. 2024;912:168308.
21. Jiang P, Jia H, Qian X, Tang T, Han Y, Zhang Z, Jiang L, Yu Z, Zheng L, Yu G, et al. Single-cell RNA sequencing reveals the immunoregulatory roles of PegIFN-α in patients with chronic hepatitis B. Hepatology. 2024;79:167–82.
22. MacParland SA, Liu JC, Ma XZ, Innes BT, Bartczak AM, Gage BK, Manuel J, Khuu N, Echeverri J, Linares I, et al. Single cell RNA sequencing of human liver reveals distinct intrahepatic macrophage populations. Nat Commun. 2018;9:4383.
23. Ramachandran P, Dobie R, Wilson-Kanamori JR, Dora EF, Henderson BEP, Luu NT, Portman JR, Matchett KP, Brice M, Marwick JA, et al. Resolving the fibrotic niche of human liver cirrhosis at single-cell level. Nature. 2019;575:512–18.
24. Butler A, Hoffman P, Smibert P, Papalexi E, Satija R. Integrating single-cell transcriptomic data across different conditions, technologies, and species. Nat Biotechnol. 2018;36:411–20.
25. Ritchie ME, Phipson B, Wu D, Hu Y, Law CW, Shi W, Smyth GK. Limma powers differential expression analyses for RNA-sequencing and microarray studies. Nucleic Acids Res. 2015;43:e47.
26. Qiu X, Mao Q, Tang Y, Wang L, Chawla R, Pliner HA. Trapnell C: reversed graph embedding resolves complex single-cell trajectories. Nat Methods. 2017;14:979–82.
27. Karmaus PWF, Chen X, Lim SA, Herrada AA, Nguyen TM, Xu B, Dhungana Y, Rankin S, Chen W, Rosencrance C, et al. Metabolic heterogeneity underlies reciprocal fates of T(H)17 cell stemness and plasticity. Nature. 2019;565:101–05.
28. Gene Ontology C: gene Ontology consortium: going forward. Nucleic Acids Res. 2015;43:D1049–1056.
29. Kanehisa M, Goto S. KEGG: kyoto encyclopedia of genes and genomes. Nucleic Acids Res. 2000;28:27–30.
30. Yu G, Wang LG, Han Y, He QY. clusterProfiler: an R package for comparing biological themes among gene clusters. OMICS. 2012;16:284–87.
31. Aibar S, Gonzalez-Blas CB, Moerman T, Huynh-Thu VA, Imrichova H, Hulselmans G, et al. SCENIC: single-cell regulatory network inference and clustering. Nat Methods. 2017;14:1083–86.
32. Fang Z, Tian Y, Sui C, Guo Y, Hu X, Lai Y, Liao Z, Li J, Feng G, Jin L, Qian K. Single-cell transcriptomics of proliferative phase endometrium: Systems analysis of cell-cell communication network using CellChat. Front Cell Dev Biol. 2022;10:919731.
33. Cui A, Huang T, Li S, Ma A, Perez JL, Sander C, Keskin DB, Wu CJ, Fraenkel E, Hacohen N. Dictionary of immune responses to cytokines at single-cell resolution. Nature. 2024;625:377–84.
34. Han JW, Kim DI, Nam HC, Chang UI, Yang JM, Song DS. Association between serum tumor necrosis factor-alpha and sarcopenia in liver cirrhosis. Clin Mol Hepatol. 2022;28:219–31.
35. Zhang T, Zhong Y, Shi Y, Feng C, Xu L, Chen Z, Sun X, Zhao Y, Sun X. Multi-omics reveals that 5-O-methylvisammioside prevention acute liver injury in mice by regulating the TNF/MAPK/NF-kappaB/arachidonic acid pathway. Phytomedicine. 2024;128:155550.
36. Shen Y, Malik SA, Amir M, Kumar P, Cingolani F, Wen J, Liu Y, Zhao E, Farris AB, Raeman R, Czaja MJ. Decreased Hepatocyte autophagy leads to synergistic IL-1beta and TNF mouse liver injury and inflammation. Hepatology. 2020;72:595–608.
37. Zhang K, Zhang MX, Meng XX, Zhu J, Wang JJ, He YF, Li YH, Zhao SC, Shi ZM, Zheng LN, et al. Targeting GPR65 alleviates hepatic inflammation and fibrosis by suppressing the JNK and NF-kappaB pathways. Mil Med Res. 2023;10:56.
38. Gaul S, Leszczynska A, Alegre F, Kaufmann B, Johnson CD, Adams LA, Wree A, Damm G, Seehofer D, Calvente CJ, et al. Hepatocyte pyroptosis and release of inflammasome particles induce stellate cell activation and liver fibrosis. J Hepatol. 2021;74:156–67.
39. Fukumoto K, Hikita H, Saito Y, Makino Y, Soma K, Kato S, Sasaki Y, Myojin Y, Sato K, Sakane S, et al. Lsecs promote MASH progression via IL-1R1-mediated chemokine production induced by macrophage-derived IL-1beta. Cell Mol Gastroenterol Hepatol. 2025;101698.
40. Shi YS, Li XX, Li HT, Zhang Y. Pelargonidin ameliorates CCl(4)-induced liver fibrosis by suppressing the ROS-NLRP3-IL-1beta axis via activating the Nrf2 pathway. Food Funct. 2020;11:5156–65.
41. Jiang P, Jia H, Qian X, Tang T, Han Y, Zhang Z, Jiang L, Yu Z, Zheng L, Yu G, et al. Single-cell RNA sequencing reveals the immunoregulatory roles of PegIFN-alpha in patients with chronic hepatitis B. Hepatology. 2024;79:167–82.
42. Bai Q, Hong X, Lin H, He X, Li R, Hassan M, Berger H, Tacke F, Engelmann C, Hu T. Single-cell landscape of immune cells in human livers affected by HBV-related cirrhosis. JHEP Rep. 2023;5:100883.
43. Albillos A, Martin-Mateos R, Van der Merwe S, Wiest R, Jalan R, Alvarez-Mon M. Cirrhosis-associated immune dysfunction. Nat Rev Gastroenterol Hepatol. 2022;19:112–34.
44. Martinez LA. Mutant p53 and ETS2, a tale of reciprocity. Front Oncol. 2016;6:35.
45. He L, Cai Q, Liang X, Xin J, Shi D, Ren K, Li Y, Chen J, Sun S, Guo B, et al. ETS2 alleviates acute-on-chronic liver failure by suppressing excessive inflammation. J Med Virol. 2023;95:e28710.
46. Sun J, Ge X, Wang Y, Niu L, Tang L, Pan S. USF2 knockdown downregulates THBS1 to inhibit the TGF-beta signaling pathway and reduce pyroptosis in sepsis-induced acute kidney injury. Pharmacol Res. 2022;176:105962.
47. Akbar SM, Abe M, Murakami H, Tanimoto K, Kumagi T, Yamashita Y, Michitaka K, Horiike N, Onji M. Macrophage migration inhibitory factor in hepatocellular carcinoma and liver cirrhosis; relevance to pathogenesis. Cancer Lett. 2001;171:125–32.
48. Wirtz TH, Reuken PA, Jansen C, Fischer P, Bergmann I, Backhaus C, Emontzpohl C, Reissing J, Brandt EF, Koenen MT, et al. Balance between macrophage migration inhibitory factor and sCD74 predicts outcome in patients with acute decompensation of cirrhosis. JHEP Rep. 2021;3:100221.
49. Korsunsky I, Millard N, Fan J, Slowikowski K, Zhang F, Wei K, Baglaenko Y, Brenner M, Loh PR, Raychaudhuri S. Fast, sensitive and accurate integration of single-cell data with Harmony. Nat Methods. 2019;16:1289–96.
50. Tran HTN, Ang KS, Chevrier M, Zhang X, Lee NYS, Goh M, Chen J. A benchmark of batch-effect correction methods for single-cell RNA sequencing data. Genome Biol. 2020;21:12.

Publisher's Note

Springer Nature remains neutral with regard to jurisdictional claims in published maps and institutional affiliations.